Vibrational Spectroscopy 120 (2022) 103379

Contents lists available at ScienceDirect

Vibrational Spectroscopy

journal homepage: www.elsevier.com/locate/vibspec

Stability of low-pressure and high-pressure $CaGa_2O_4$ polymorphs at elevated temperatures: Raman spectroscopic study

Weihong Xue [a], Xinyu Lei [a,b], Yungui Liu [c], Xiang Wu [c], Shuangmeng Zhai [a,*]

[a] Key Laboratory of High-temperature and High-pressure Study of the Earth's Interior, Institute of Geochemistry, Chinese Academy of Sciences, Guiyang 550081, China
[b] University of Chinese Academy of Sciences, Beijing 100049, China
[c] State Key Laboratory of Geological Processes and Mineral Resources, China University of Geosciences, Wuhan 430074, China

ARTICLE INFO

Keywords:
$CaGa_2O_4$
Raman spectra
High temperature
Phase transition

ABSTRACT

The temperature-dependent Raman spectra of low-pressure and high-pressure $CaGa_2O_4$ have been investigated from 80 to 1173 K at ambient pressure. For the low-pressure $CaGa_2O_4$, it is stable and no phase transition was observed in this study. But a phase transition for the high-pressure $CaGa_2O_4$ was observed at 923 K into low-pressure $CaGa_2O_4$, and this temperature-induced phase transition is irreversible. All the observed Raman active bands of low-pressure and high-pressure $CaGa_2O_4$ showed linear temperature dependence with different slopes. The quantitative temperature dependences of Raman bands are $-3.04 \times 10^{-2} \sim -0.05 \times 10^{-2}$ and $-2.76 \times 10^{-2} \sim 2.13 \times 10^{-2}$ cm^{-1} K^{-1} for low-pressure and high-pressure $CaGa_2O_4$, respectively.

1. Introduction

Based on their different crystal structural, physical and chemical properties and broad applications, oxometallates with composition AM_2O_4 have been widely investigated [1]. $CaGa_2O_4$, a member of oxometallates, has been used as a matrix for fluorescent materials with various dopants [2–10]. Since it is with a low dielectric constant, $CaGa_2O_4$ can be adopted as a microwave dielectric ceramic [11]. In previous studies, three $CaGa_2O_4$ polymorphs have been reported including low-pressure (LP-$CaGa_2O_4$), high-pressure (HP-$CaGa_2O_4$) and high-temperature (HT-$CaGa_2O_4$) forms [12–14]. The crystal structures of these polymorphs were refined [15–18]. LP- and HP-$CaGa_2O_4$ are in the orthorhombic with different space groups of $Pna2_1$ and $Pnam$, whereas HT-$CaGa_2O_4$ is in the monoclinic with space group of $P2_1/c$. According to their crystal structures, HP- and HT-$CaGa_2O_4$ may also accommodate some rare earth elements and have potential applications for fluorescent materials. LP-$CaGa_2O_4$ can be synthesized at high-temperature [12], and HP-$CaGa_2O_4$ can be obtained by high-pressure and high-temperature experiments [13]. But it is difficult to obtain pure HT-$CaGa_2O_4$ [14] since the synthetic temperature of HT-$CaGa_2O_4$ is very close to its melting point [12]. The crystal structures of LP- and HP-$CaGa_2O_4$ were shown in Fig. 1.

In previous studies, the phase boundary between LP- and HP-$CaGa_2O_4$ was experimentally determined [13], and the temperature boundary between LP- and HT-$CaGa_2O_4$ was constrained at about 1350 °C under ambient pressure [14]. However, the physical and chemical properties of $CaGa_2O_4$ polymorphs have not been well investigated. In this study, the stability and vibrational features of synthetic LP- and HP-$CaGa_2O_4$ were studied at elevated temperatures (from 80 to 1173 K) and ambient pressure by adopting using Raman spectroscopy. A temperature-induced irreversible phase transition for HP-$CaGa_2O_4$ was observed at 923 K to LP-$CaGa_2O_4$. The temperature-dependent Raman active modes of LP-$CaGa_2O_4$ and HP-$CaGa_2O_4$ polymorphs were quantitatively analyzed.

2. Experimental details

High-purity LP-$CaGa_2O_4$ was prepared by a solid-state reaction from $CaCO_3$ and Ga_2O_3. Reagent-grade $CaCO_3$ (99.99%, Alfa Aesar) and Ga_2O_3 (99.99%, Alfa Aesar) powders were mixed in the proportion corresponding to the $CaGa_2O_4$ stoichiometry, and the mixture was ground sufficiently and pressed into pellets with a diameter of 8 mm under uniaxial pressure of 20 MPa. The pellets were sintered at 1473 K in a furnace for 72 h, during which the sample was cooled, ground, and heated three times. According to the reported phase diagram [13], HP-$CaGa_2O_4$ phase was synthesized from LP-$CaGa_2O_4$ powder at 4 GPa and 1273 K for 5 h. The sintered and synthesized LP- and HP-$CaGa_2O_4$ phases were confirmed as single phases by using an Empyrean

* Correspondence to: Institute of Geochemistry, Chinese Academy of Sciences, Guiyang 550081, China.
E-mail address: zhaishuangmeng@mail.gyig.ac.cn (S. Zhai).

https://doi.org/10.1016/j.vibspec.2022.103379
Received 17 March 2022; Received in revised form 13 April 2022; Accepted 24 April 2022
Available online 4 May 2022

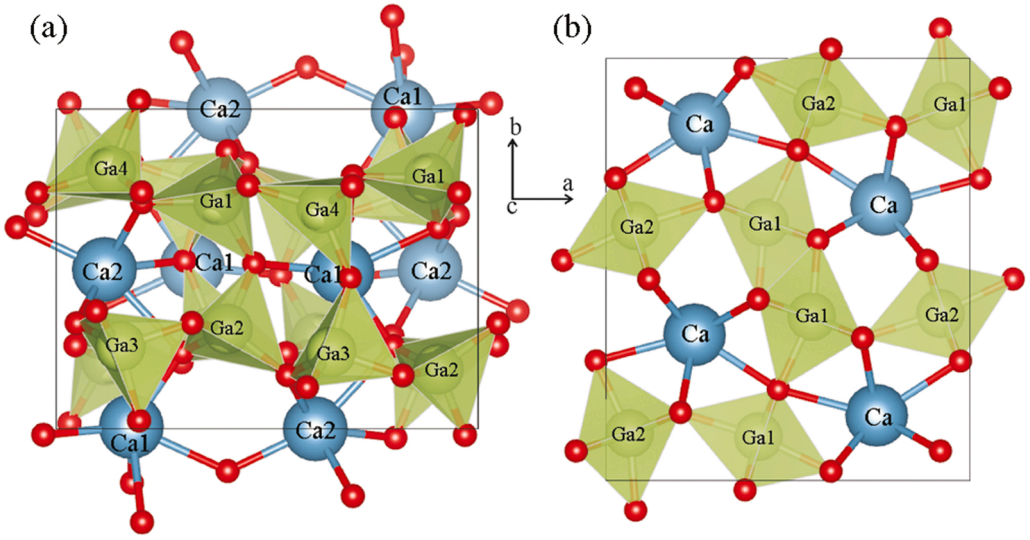

Fig. 1. The crystal structures of low-pressure $CaGa_2O_4$ (a) and high-pressure (b) $CaGa_2O_4$ polymorphs.

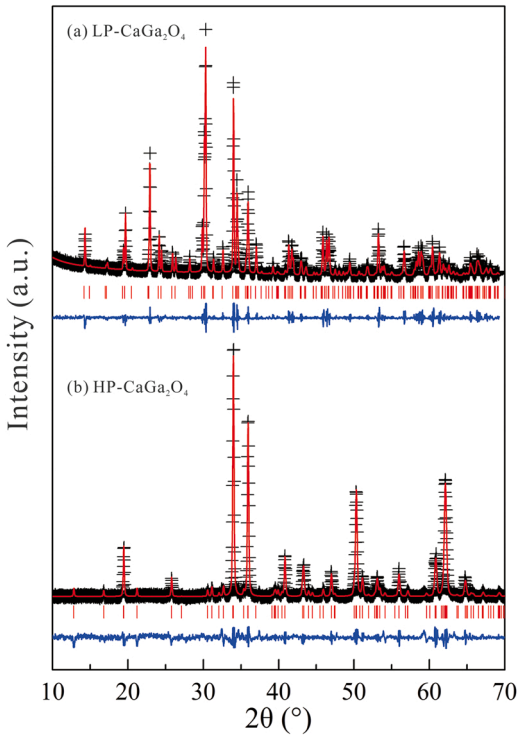

Fig. 2. Refined X-ray diffraction patterns of low-pressure $CaGa_2O_4$ (a) and high-pressure $CaGa_2O_4$ (b) $CaGa_2O_4$ obtained at ambient conditions. Observed (black crosses), calculated (red line) and difference (bottom blue curve) powder XRD pattern determined by Rietveld analysis.

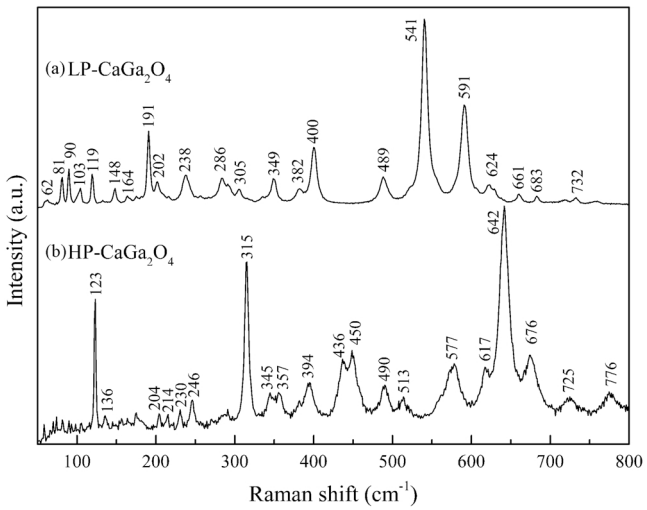

Fig. 3. Raman spectra of low-pressure $CaGa_2O_4$ (a) and high-pressure (b) $CaGa_2O_4$ at ambient conditions.

diffractometer with Cu Kα radiation operated at 40 kV and 200 mA. The collected XRD patterns of both LP- and HP-$CaGa_2O_4$ were refined using EXPGUI/GSAS program, and the results were shown in Fig. 2.

Raman spectra of LP- and HP-$CaGa_2O_4$ at various temperatures and ambient pressure were collected in the wavenumber range of 50 ~ 1000 cm^{-1}. The method was similar to those in our previous studies [19, 20]. A Raman spectrometer (Horiba LabRam HR Evolution) equipped with an 1800 gr/mm grating was adopted, and it was calibrated by plasma and neon emission lines with a high spectral resolution of 1 cm^{-1}. The exciting source is YAG: Nd^{3+} laser with a wavelength of 532 nm and a power of 20 mW for the samples. The laser beam was focused by an SLM Plan 20 × Olympus microscope objective to collect the scattered light. Small pieces of synthesized samples were put on a sapphire or silica window for the high-temperature or low-temperature Raman spectroscopic measurements, respectively. The sapphire window was put into an alumina chamber in Linkam TS 1500 for heating from room temperature to 1173 K, and the silica window was placed at the center of a small silver block in THMSG 600 for freezing from 80 K to room temperature. In high-temperature measurements, a resistance heater with a water cooling system was used and temperature was monitored by an S-type thermocouple. In low-temperature measurements, liquid nitrogen was pumped in the silver block and a resistance heater opposes the cooling effect of the nitrogen to reach the target temperature. The heating or cooling systems have been calibrated by observing phase changes in synthetic fluid inclusions placed into the crucibles. In all measurements, the temperature control unit is automatically changed at a constant rate of 10 K/min and can be programmed to hold at desired temperatures. For thermal equilibrium, the Raman spectra were collected after keeping at a desired temperature for 10–15 min. The accumulation duration for each spectrum was 60 s, and the final spectrum was the average of three measurements. All Raman spectra were analyzed by using the PeakFit program (SPSS Inc.,

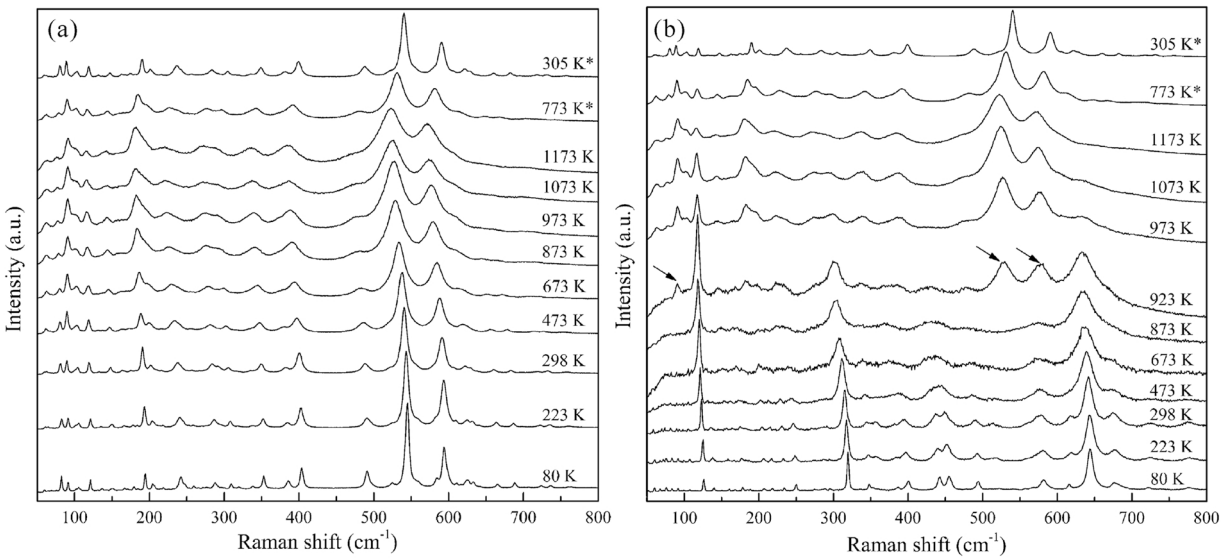

Fig. 4. Typical Raman spectra of low-pressure $CaGa_2O_4$ (a) and high-pressure $CaGa_2O_4$ (b) at different temperatures. The temperatures with * symbols represent cooling steps. The arrows indicate appearance of new Raman peaks during heating.

Chicago) to obtain the shifts of bands.

3. Results and discussion

3.1. Raman spectrum of HP-$CaGa_2O_4$ at ambient conditions

In previous studies [11,21], the vibrational spectrum of LP-$CaGa_2O_4$ at ambient conditions was reported and interpreted. The obtained Raman spectrum of LP-$CaGa_2O_4$ in the present study at ambient conditions, as shown in Fig. 3, is consistent with previous studies [11,21]. However, there is no Raman spectrum of HP-$CaGa_2O_4$ in literatures.

According to the factor group analysis using symmetry-adapted modes [22] and based on the *Pnam* space group, the Raman active modes of HP-$CaGa_2O_4$ can be predicted as following:

$$\Gamma = 14A_g + 7B_{1g} + 14B_{2g} + 7B_{3g}.$$

Therefore, totally 42 Raman vibrational modes are predicted for HP-$CaGa_2O_4$. Raman spectrum of HP-$CaGa_2O_4$ at ambient conditions is also shown in Fig. 3. Obviously, the numbers of observed Raman vibrations for HP-$CaGa_2O_4$ are fewer than the theoretically predicted, which is due to some undetected weak Raman active modes and/or overlapping.

The Raman spectrum of HP-$CaGa_2O_4$ was firstly reported in the present study, which shows three strongest modes at 642, 315 and 123 cm^{-1} and some weak peaks. It is difficult to assign those different peaks of HP-$CaGa_2O_4$ without theoretical simulation though the Raman active modes of some isostructural compounds (e.g., $CaFe_2O_4$ [23], $CaAl_2O_4$ and $MgAl_2O_4$ [24]) were assigned in previous studies. In the crystal structure of HP-$CaGa_2O_4$, all Ca atoms are in eight-coordination and two kinds of Ga atoms are in six-coordination, and both corner-sharing and edge-sharing GaO_6 octahedra exist [18]. According to previous Raman spectroscopic studies on some gallates containing GaO_6 octahedra [25,26], the most intense Raman band of HP-$CaGa_2O_4$ at 642 cm^{-1} corresponds to symmetric stretching mode of GaO_6, bands at 725 and 776 cm^{-1} can be assigned to anti-symmetric stretching vibrations of GaO_6, band at 315 cm^{-1} is related to the O-Ga-O bending vibration. And the low-wavenumber modes below 300 cm^{-1} are originated from the displacements of the apical oxygen and Ca atoms [27]. Further theoretical calculation is required for assign the different Raman active modes of HP-$CaGa_2O_4$.

3.2. Stability of LP- and HP-$CaGa_2O_4$

The representative Raman spectra of LP- and HP-$CaGa_2O_4$ at different temperatures are illustrated in Fig. 4. Obviously, the Raman bands of both LP- and HP-$CaGa_2O_4$ gradually become broad and shift towards lower wavenumbers during heating. It is reasonable since bond length increases due to thermal expansion. Longer bond lengths imply weaker bonds, i.e., smaller force constant, and thus lower vibrational wavenumber according to Hooke's law.

It is clear that LP-$CaGa_2O_4$ is stable in the present temperature range, as shown in Fig. 4(a). Up to 1173 K, no phase transition was observed for LP-$CaGa_2O_4$ though some Raman peaks become weak and undistinguished during heating. The Raman spectrum at 305 K after cooling from 1173 K is same as the initial Raman spectrum of LP-$CaGa_2O_4$ shown in Fig. 3 at ambient conditions.

Obviously, new peaks begin to appear in the Raman spectrum of HP-$CaGa_2O_4$ at 923 K, as marked by arrows in Fig. 4(b), which indicates that a temperature-induced phase transition occurs. With further increasing temperature, the typical Raman bands of HP-$CaGa_2O_4$ become weak and disappear at 1173 K. It seems that HP-$CaGa_2O_4$ and its phase transition product can coexist in a temperature range. Kinetics may be another reason to explain the coexisting of HP-$CaGa_2O_4$ and its phase transition product. The Raman spectrum at 305 K after cooling from 1173 K is totally different from the initial Raman spectrum of HP-$CaGa_2O_4$ shown in Fig. 3 at ambient conditions, which indicates that the temperature-induced phase transition is irreversible. Compared the Raman spectra, it is clearly noted that the final obtained product is LP-$CaGa_2O_4$. As mentioned above, both HP- and LP-$CaGa_2O_4$ belong to orthorhombic structure but in different space groups. At ambient conditions, HP-$CaGa_2O_4$ contains CaO_8 and GaO_6 polyhedra with average bond lengths of 2.426 and 2.013 Å for Ca-O and Ga-O [18], whereas LP-$CaGa_2O_4$ contains CaO_7, GaO_4 and GaO_5 polyhedra with average bond lengths of 2.503 and 1.902 Å for Ca-O and Ga-O [16]. Therefore, during the temperature-induced phase transformation from HP-$CaGa_2O_4$ (space group of *Pnam*) into LP-$CaGa_2O_4$ (space group of $Pna2_1$), all coordinated numbers of cations and Ga-O bond lengths decrease, but the Ca-O bong lengths increase. It indicates that the observed temperature-induced irreversible phase transition of HP-$CaGa_2O_4$ is of the first-order. Further investigation is necessary to clarify the mechanism of temperature-induced phase transformation from HP-$CaGa_2O_4$ into LP-$CaGa_2O_4$.

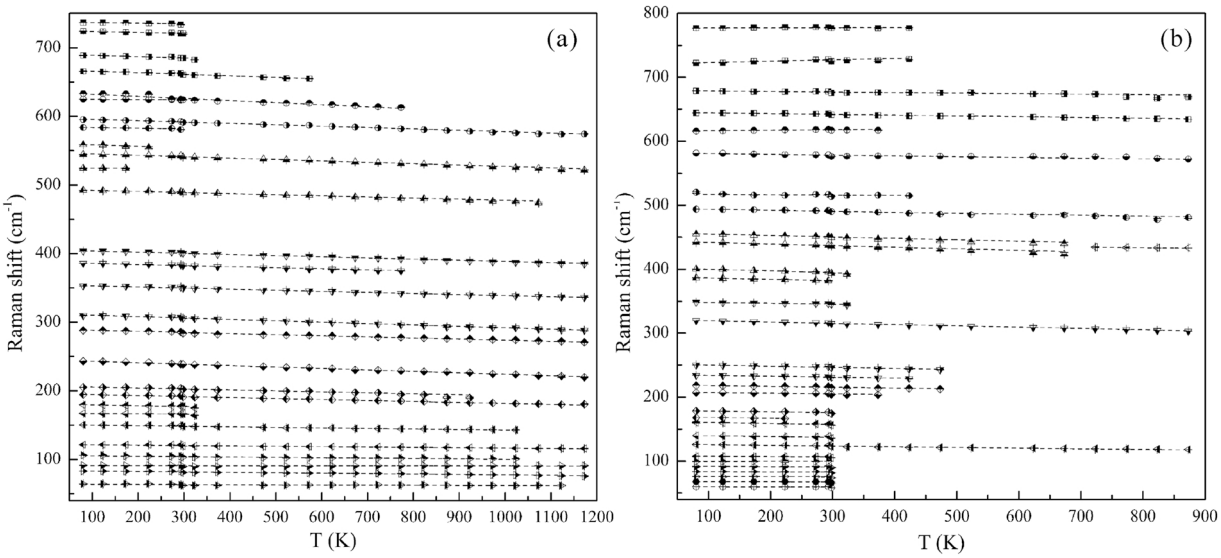

Fig. 5. Temperature dependence of the Raman bands of low-pressure $CaGa_2O_4$ (a) and high-pressure $CaGa_2O_4$ (b) at ambient pressure.

Table 1
Constants determined in $\nu_i = a_i + b_i T$ at ambient pressure for $CaGa_2O_4$.

LP-$CaGa_2O_4$			HP-$CaGa_2O_4$		
Peak No.	a_i	$-b_i \times 10^2$	Peak No.	a_i	$-b_i \times 10^2$
1	63.8(3)	0.17(5)	1	60.0(3)	0.06(8)
2	83.6(2)	0.61(5)	2	67.9(2)	0.09(12)
3	90.8(3)	0.05(5)	3	75.9(3)	0.19(18)
4	105.7(3)	0.54(5)	4	84.1(6)	0.34(28)
5	121.8(1)	0.54(3)	5	92.4(9)	0.51(41)
6	150.8(2)	0.82(4)	6	99.3(1)	-0.21(5)
7	167.4(2)	0.45(17)	7	108.1(6)	0.50(29)
8	180.5(4)	1.16(22)	8	126.8(3)	1.07(8)
9	195.9(2)	1.44(6)	9	140.8(5)	1.29(29)
10	206.8(3)	1.38(9)	10	161.8(5)	1.55(24)
11	245.1(2)	2.11(5)	11	168.9(2)	0.10(17)
12	289.9(3)	1.63(6)	12	179.4(4)	1.16(26)
13	312.2(2)	2.02(7)	13	208.2(5)	0.10(23)
14	354.4(2)	1.57(4)	14	219.3(3)	1.26(13)
15	387.1(2)	1.54(8)	15	235.5(3)	1.34(14)
16	405.3(2)	1.67(6)	16	251.7(3)	1.71(17)
17	493.8(2)	1.59(7)	17	321.6(2)	2.03(9)
18	524.4(1)	0.13(4)	18	349.2(3)	1.20(15)
19	547.3(2)	2.02(6)	19	388.1(3)	1.95(17)
20	560.4(9)	2.05(30)	20	402.8(4)	2.76(26)
21	584.5(3)	0.91(18)	21	444.4(2)	2.45(12)
22	597.6(2)	1.98(6)	22	457.0(2)	2.18(11)
23	625.2(2)	0.35(14)	23	495.4(3)	0.70(26)
24	635.2(2)	3.04(21)	24	518.0(20)	0.68(71)
25	668.0(5)	2.24(17)	25	582.2(4)	1.22(14)
26	690.6(8)	1.80(35)	26	615.5(4)	-0.87(19)
27	725.1(1)	1.42(8)	27	645.6(3)	1.16(11)
28	737.3(3)	0.84(17)	28	679.2(4)	0.78(16)
			29	721.0(9)	-2.13(38)
			30	777.2(5)	-1.63(20)

ai is in cm^{-1}, T in K, and the constant bi in cm^{-1} K^{-1}.

3.3. Temperature-dependent Raman spectra of LP- and HP-$CaGa_2O_4$

The wavenumber shifts of the Raman bands of LP-$CaGa_2O_4$ as a function of temperature up to 1173 K are shown in Fig. 5(a). Totally 28 bands could be reliably indentified for LP-$CaGa_2O_4$. These bands all show a linear decrease in Raman shift with increasing temperature. The temperature dependences for each of the observed bands are given in Table 1, ranging from -3.04×10^{-2} to -0.05×10^{-2} cm^{-1} K^{-1}.

The Raman shift versus temperature plot of HP-$CaGa_2O_4$ is illustrated in Fig. 5(b). Totally 30 Raman active bands could be reliably indentified as a function of temperature. The Raman shifts of all modes in HP-$CaGa_2O_4$ change linearly and continuously with temperature, and the slopes are different for different modes. The temperature dependences for each of the observed bands are also listed in Table 1, ranging from -2.76×10^{-2} to 2.13×10^{-2} cm^{-1} K^{-1}. It is noted that HP-$CaGa_2O_4$ shows some positive temperature dependences of some Raman active bands, which means that the Raman shifts of these modes increase with increasing temperature. Indeed, such positive temperature dependence of Raman shift was reported in α-$Mg_2P_2O_7$ [28], HT-$Ca_2AlSiO_{5.5}$ [29], SiO_2 [30] and GeO_2 [31]. The reason is not clear. It may be related to the band evolution under high temperatures.

4. Conclusions

By using Raman spectroscopic measurements, the stability and vibrations of low-pressure and high-pressure $CaGa_2O_4$ gallates were investigated in the temperature region of 80–1173 K at ambient pressure. No phase transition was observed for low-pressure $CaGa_2O_4$ up to 1173 K, but an irreversible temperature-induced phase transformation begins to occur for high-pressure $CaGa_2O_4$ at 923 K to form a low-pressure $CaGa_2O_4$ phase. The Raman wavenumbers of all observed vibrations for low-pressure and high-pressure $CaGa_2O_4$ polymorphs continuously and linearly change with increasing temperature. The temperature coefficients of all Raman active modes for the two phases were quantitatively determined, ranging from -3.04×10^{-2} to -0.05×10^{-2} cm^{-1} K^{-1} for low-pressure $CaGa_2O_4$ and -2.76×10^{-2} to 2.13×10^{-2} cm^{-1} K^{-1} for high-pressure $CaGa_2O_4$.

CRediT authorship contribution statement

Weihong Xue: Investigation, Writing – original draft, Funding acquisition. **Xinyu Lei**: Data curation. **Yungui Liu:** Data curation. **Xiang Wu**: Methodology, Resources. **Shuangmeng Zhai**: Conceptualization, Writing – review & editing, Funding acquisition.

Declaration of Competing Interest

The authors declare that they have no known competing financial interests or personal relationships that could have appeared to influence the work reported in this paper.

Acknowledgements

This work was financially supported by the National Natural Science Foundation of China (Grant No. 41872045) and Chinese Academy of Sciences (Grant No. 132852KYSB20200011).

References

[1] H. Müller-Buschbaum, J. Alloys Compds. 349 (2003) 49–104.
[2] P.J. Saines, M.M. Elcombe, B.J. Kennedy, J. Solid State Chem 179 (2006) 613–622.
[3] D. Ye, Z. Hu, W. Zhang, Y. Cui, L. Luo, Y. Wang, Opt. Mater. 36 (2014) 1879–1882.
[4] M. Rai, S.K. Singh, K. Mishra, R. Shankar, R.K. Srivastava, S.B. Rai, J. Mater. Chem. C 2 (2014) 7918–7926.
[5] L.L. Noto, S.K.K. Shaat, D. Poelman, M.S. Dhlamini, B.M. Mothudi, H.C. Swart, Ceram. Int. 42 (2016) 9779–9784.
[6] S. Wang, W. Chen, D. Zhou, J. Qiu, X. Xu, X. Yu, J. Am. Ceram. Soc. 100 (2017) 3514–3521.
[7] M. Rai, K. Mishra, S.B. Rai, P. Morthekai, Mater. Res. Bull. 105 (2018) 192–201.
[8] A. Ul'ana, V.A. Vorob'ev, A.P. Mar'in, Mod. Electron. Mater. 6 (2020) 31.
[9] Y. Wang, P. Feng, S. Ding, S. Tian, Y. Wang, Inorg. Chem Front 8 (2021) 3748–3759.
[10] K. Kniec, W. Piotrowski, K. Ledwa, L.D. Carlos, L. Marciniak, J. Mater. Chem. C 9 (2021) 517–527.
[11] B. Liu, K. Sha, M.F. Zhou, K.X. Song, Y.H. Huang, C.C. Hu, J. Eur. Ceram. Soc. 41 (2021) 5170–5175.
[12] J. Jeevaratnam, F.P. Glasser, J. Am. Ceram. Soc. 44 (1961) 563–566.
[13] S. Ito, K. Suzuki, M. Inagaki, S. Naka, Mater. Res. Bull. 15 (1980) 925–932.
[14] F. Jiang, P. Jiang, M. Yue, W. Gao, R. Cong, T. Yang, J. Solid State Chem 254 (2017) 195–199.
[15] J. Jeevaratnam, F.P. Glasser, L.D. Glasser, Z. Krist. -Cryst. Mater. 118 (1963) 257–262.
[16] H.J. Deiseroth, H. Müller-Buschbaum, Z. Anorg. Allg. Chem. 396 (1973) 157–164.
[17] H.J. Deiseroth, H. Müller-Buschbaum, Z. Anorg. Allg. Chem. 402 (1973) 201–205.
[18] B. Lazić, V. Kahlenberg, J. Konzett, Z. Anorg. Allg. Chem. 631 (2005) 2411–2415.
[19] M. Jia, K. Zhai, M. Gao, W. Wen, Y. Liu, X. Wu, S. Zhai, Vib. Spectrosc. 106 (2020), 103005.
[20] X. Hu, K. Zhai, M. Jia, Y. Liu, X. Wu, W. Wen, W. Xue, S. Zhai, Spectrochim. Acta A 269 (2022) 120762..
[21] H. Zheng, Z. Zhang, J. Zhou, S. Yang, J. Zhao, Appl. Phys. A 108 (2012) 465–473.
[22] E. Kroumova, M.I. Aroyo, J.M. Perez Mato, A. Kirov, C. Capillas, S. Ivantchev, H. Wondratschek, Phase Transit. 76 (2003) 155–170.
[23] N. Kolev, M.N. Iliev, V.N. Popov, M. Gospodinov, Solid State Commun. 128 (2003) 153–155.
[24] H. Kojitani, D.M. Többens, M. Akaogi, Am. Mineral. 98 (2013) 197–206.
[25] V. Monteseguro, P. Rodríguez-Hernández, R. Vilaplana, F.J. Manjón, V. Venkatramu, D. Errandonea, V. Lavín, A. Muñoz, J. Phys. Chem. C 118 (2014) 13177–13185.
[26] K. Papagelis, J. Arvanitidis, E. Vinga, D. Christofilos, G.A. Kourouklis, H. Kimura, S. Ves, J. Appl. Phys. 107 (2010), 113504.
[27] R. Sopracase, G. Gruener, E. Olive, J. Soret Phys. B 405 (2010) 45–52.
[28] W. Xue, K. Zhai, X. Wang, W. Wu, S.Zhai Wen, Spectrochim. Acta A 273 (2022), 121076.
[29] S. Zhai, K. Zhai, H. Wang, X. Wu, W. Xue, Vib. Spectrosc. 103 (2019), 102935.
[30] L. Liu, T.P. Mernagh, W.O. Hibberson, Phys. Chem. Miner. 24 (1997) 396–402.
[31] T.P. Mernagh, L. Liu, Phys. Chem. Miner. 24 (1997) 7–16.